ACS Photonics

Article

pubs.acs.org/journal/apchd5

Phase Bifurcation and Zero Reflection in Planar Plasmonic Metasurfaces

Chen Yan, T. V. Raziman, and Olivier J. F. Martin*

Nanophotonics and Metrology Laboratory, Swiss Federal Institute of Technology (EPFL), CH-1015 Lausanne, Switzerland

Supporting Information

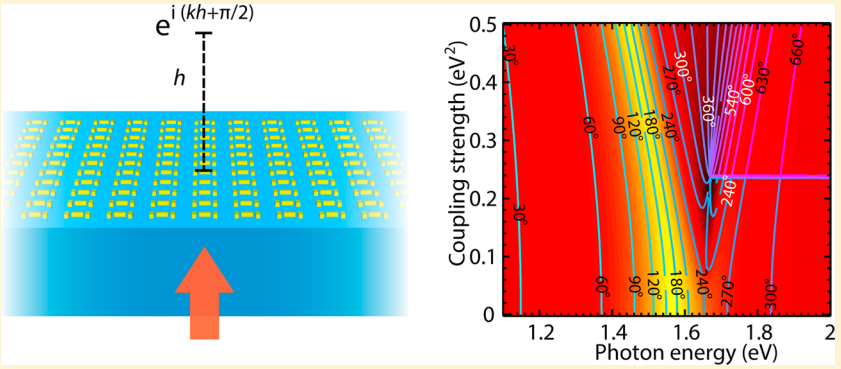

ABSTRACT: We introduce a general formalism combining the coupled oscillator model with the transfer matrix method to analyze and engineer the phase of the light reflected from a Fano-resonant metasurface. This method accounts for periodicity and the presence of substrates, and we demonstrate that these factors can be used to tune the reflected phase at will. Utilizing these effects and adjusting the coupling strength of the underlying unit cell, we achieve zero reflection at the dark resonance of the metasurface. We show that the resulting phase singularity can dramatically increase the sensitivity of phase-based detection schemes. The phase bifurcation unveiled in this work can be used to design plasmonic metasurfaces that explore the unusual phase behavior of light.

KEYWORDS: *plasmonics, metasurfaces, phase singularity*

Light scattering from plasmonic metasurfaces has received significant attention over the past few years, leading to a broad range of applications such as wavefront engineering, molecular identification, spectroscopy, and enhanced nonlinear generation.[1−13] The functionality of a metasurface depends on both the near-field and far-field responses of the unit cell that composes it, which usually consists of multipart plasmonic or dielectric nanostructures. Plasmonic nanoparticles and optical antennas that support Lorentzian resonances can be modeled as classical oscillators.[14−16] In turn, the response of compound structures can be described using coupled mode theory for the harmonic modes.[17−21] Although these models have been used to successfully describe the light intensity spectra, another fundamental property of light, phase, has not been well analyzed, especially in the case of periodic structures.

Retrieving both the phase and the amplitude information is important for applications such as high precision metrology and ellipsometric sensing.[22−26] Techniques based on rapid spatial phase changes have been achieved in various plasmonic systems used to improve the performance of optical sensors.[27−29] However, frequency-dependent phase variations are correlated with resonance line widths, and intrinsic losses in metals result in broad line widths and slow spectral variations.[14,30,31] Optical Fano resonances utilizing dark modes are employed for reducing the radiative loss of localized surface plasmon resonances (LSPRs) in both individual nanostructures and periodic arrays.[12,15,20,32−36]

When substrate effects are taken into consideration, the phase is no longer a property of the plasmonic resonances alone, but also depends on the interference with light reflected from the interfaces and the resulting asymmetry in the light propagation direction. For example, the presence of a substrate has been shown to suppress lattice resonances[37,38] and induce symmetry breaking with Fano resonances.[39,40] The substrate also modifies the spatial distribution of the near-field in the different media, which maximizes the light−matter interaction[41,42] and enhances the sensitivity of biosensors.[43−45]

In this work, we study the influence of the substrate on the phase for periodic structures and unveil the phenomenon of phase bifurcation in a Fano-resonant metasurface, which enables extremely rapid phase modulation of the reflected light without having to further reduce the plasmonic losses in the system. We start by analyzing the reflected light from a two-dimensional (2D) subwavelength array of dipoles and show that it exhibits a $\pi/2$ phase shift compared to the scattering

Received: November 16, 2016
Published: March 10, 2017

DOI: 10.1021/acsphotonics.6b00914
ACS Photonics 2017, 4, 852−860

from an individual dipole. The classical oscillator model is modified to include this phase change. We then generalize it for a periodic array of nanostructures supporting dark resonances, by modeling the unit cell as two coupled oscillators. Then we utilize the transfer matrix method (TMM) to incorporate the effect of the substrate. We show that zero reflection at the dark resonance can be achieved by adjusting the coupling strength and results in a phase bifurcation. Finally, we propose phase-based sensing near the bifurcation region in order to improve the detection limit of refractive index changes and achieve ultrahigh sensitivity.

DISCUSSION

Phase Difference in Scattering between Individual and Periodic Scatterers. We assume the time dependence $e^{-i\omega t}$ for the electromagnetic field throughout. Let us first consider an infinite homogeneous space with permittivity ε and permeability μ; the scattering from a plasmonic nanostructure can be calculated in the dipolar approximation using the Green's tensor $\bar{\mathbf{G}}(\mathbf{r},\mathbf{r}_0)$.[46] Consider a single dipole at a position $r_0 = (0,0,0)$ that exhibits a dipole moment $\mathbf{p} = (p_x,0,0)$ oscillating with angular frequency ω. The electric field at the location $\mathbf{r} = (0,0,h)$ with $h \gg \lambda$ can be written as

$$\begin{aligned}\mathbf{E}^{\text{single}}(\omega,\mathbf{r}) &= \mu\omega^2\bar{G}(\mathbf{r},\mathbf{r}_0)\cdot\mathbf{p}\\ &= \mu\omega^2 p_x\left(1+\frac{\partial_x\partial_x}{k^2}\right)\frac{e^{ikh}}{4\pi h}\hat{\mathbf{x}}\\ &= \frac{\mu}{4\pi h}\omega^2 p_x e^{ikh}\hat{\mathbf{x}}\end{aligned} \tag{1}$$

where $k^2 = \omega^2\varepsilon\mu$ corresponds to the wave vector in the background medium, and the term e^{ikh} denotes the phase change with propagation.

Now we consider a 2D infinite array consisting of identical dipoles with dipole moments given by $\mathbf{p} = (p_x,0,0)$ and subwavelength periodicities in x- and y-directions equal to $\Gamma_x = a$ and $\Gamma_y = b$. We are interested in the total scattered light at the location $\mathbf{r} = (0,0,h)$ with $h \gg a,b,\lambda$. The electric field at this point is the sum of scattered fields from all the dipoles in the array,

$$\begin{aligned}\mathbf{E}^{\text{array}}(\omega,\mathbf{r}) &= \sum_{n=-\infty}^{\infty}\sum_{m=-\infty}^{\infty}\mu\omega^2\bar{\mathbf{G}}(\mathbf{r},\mathbf{r}_{nm})\cdot\mathbf{p}\\ &= \mu\omega^2 p_x\left(1+\frac{\partial_x\partial_x}{k^2}\right)\sum_{n=-\infty}^{\infty}\sum_{m=-\infty}^{\infty}\frac{e^{ikr}}{4\pi r}\hat{\mathbf{x}}\end{aligned} \tag{2}$$

where $r = \sqrt{(na)^2+(mb)^2+h^2}$ is the distance between the specific dipole and the observation point. As a consequence of symmetry, the y- and z-components of the field cancel out. According to the previous assumption $h \gg a,b$ and in the limit when $h \to \infty$, the asymptote of the above summation is equivalent to integration over x and y. In addition, since the integral is invariant in x, the partial derivative term vanishes. Then, we perform the polar coordinate transformation and rewrite the remaining x-component of the field as

$$\begin{aligned}E_x^{\text{array}}(\omega,\mathbf{r}) &= \frac{\omega^2\mu p_x}{4\pi}\int_{x=-\infty}^{\infty}\int_{y=-\infty}^{\infty}\frac{e^{ikr}}{r}\frac{dx}{a}\frac{dy}{b}\\ &= \frac{\omega^2\mu p_x}{4\pi}\cdot\frac{2\pi}{ab}\int_{\rho=0}^{\infty}\frac{e^{ik\sqrt{\rho^2+h^2}}}{\sqrt{\rho^2+h^2}}\rho d\rho\\ &= \frac{-i\omega p_x\sqrt{\mu}}{2ab\sqrt{\varepsilon}}[e^{ikr}]_h^{\infty}\end{aligned} \tag{3}$$

Equation 3 converges only when assuming that there is a small loss in the space (i.e., k has a small imaginary part),[47] and one can then find the analytical expression for the electric field

$$E_x^{\text{array}}(\omega,\mathbf{r}) = \frac{i\sqrt{\mu}}{2ab\sqrt{\varepsilon}}\omega p_x e^{ikh} = \frac{\sqrt{\mu}}{2ab\sqrt{\varepsilon}}\omega p_x e^{i(kh+\pi/2)} \tag{4}$$

Similar to eq 1, the total scattered field from a 2D array is described by the multiplication of a propagation term e^{ikh} and a factor depending on the dipole moment. However, the field has an additional phase of $\pi/2$ and a different frequency-dependent expression compared to the scattered field of a single dipole. Physically, the effective number of elements that interfere constructively at a specific point is proportional to the wavelength. This results in the reduction of the exponent of the frequency dependence from ω^2 in eq 1 to ω in eq 4. The additional phase shift is also due to the interference of all the dipoles in the plane.

Figure 1 illustrates such an effect in plasmonic systems. We simulate a gold nanorod with dimensions 110 × 40 × 40 nm^3

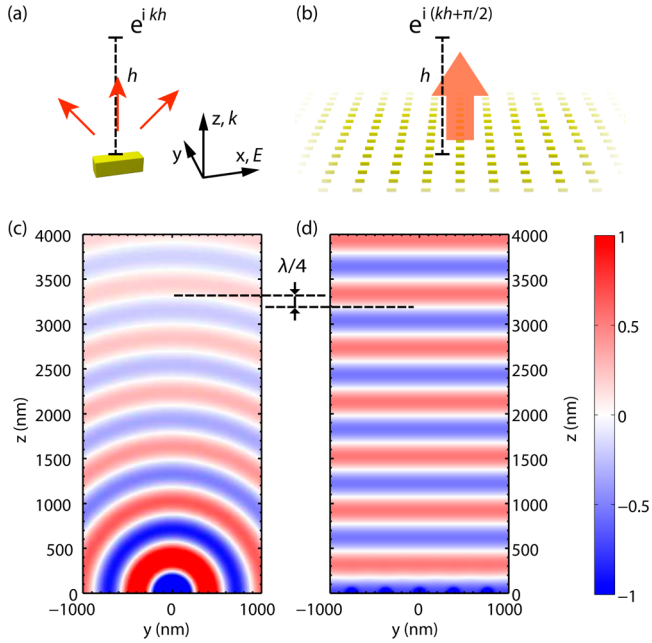

Figure 1. Schematic of (a) a single nanorod, and (b) an infinite 2D array of nanorods, showing the illumination condition. Calculated x-component of the scattered electric field in the yz-plane for (c) the single nanorod and (d) the periodic array. The field plots are for λ = 740 nm and exhibit a phase difference of $\pi/2$ (corresponding to $\lambda/4$) between the two wavefronts.

excited by an x-polarized plane wave using the surface integral equation (SIE) either for an individual nanorod[48,49] or for an infinite array of nanorods[50] considering a Drude model for the gold permittivity (ω_{plasma} = 8.95 eV, ε_∞ = 9.5, and γ = 0.691 eV).[51] The refractive index of the homogeneous surrounding

DOI: 10.1021/acsphotonics.6b00914
ACS Photonics 2017, 4, 852−860

medium, $\bar{n} = (n_{air}n_{glass})^{1/2} = 1.225$, corresponds to the geometric mean of the indices of air and glass. This value is chosen in order to obtain a similar resonance frequency when glass substrates are included in the simulation later. For a wavelength equal to 740 nm, the x-component of the field in the yz-plane is shown in Figure 1c. Similarly, we simulate a 2D array of identical nanorods with periodicity $\Gamma_x = \Gamma_y = 400$ nm. The resulting E_x field component in the yz-plane at the same wavelength is shown in Figure 1d. Comparing panels c and d in Figure 1, we observe a mismatch of $\lambda/4$ between the two wavefronts, which indicates the additional phase delay of $\pi/2$ produced by the periodic structure. This somewhat unexpected effect has to be considered while designing planar plasmonic surfaces and must be included in the coupled oscillator model that will be presented in the following.

Oscillator Model for Plasmonics. In terms of spectral response, plasmonic resonances exhibit a broad Lorentzian line shape, which is analogous to that of a classical damped oscillator. For example, a dipole resonance supported by a single gold nanorod can be described by the motion of a charge cloud with intrinsic restoring force and loss, driven by an external harmonic force.[52] The differential equation of the dynamic motion is

$$\ddot{x} + \gamma\dot{x} + \omega_0^2 x = E_0 e^{-i\omega t} + \alpha\dddot{x} \tag{5}$$

where x is the oscillation amplitude of the charge cloud, ω_0 is the eigenfrequency of the oscillator in the absence of damping, γ is the internal damping parameter, E_0 and ω are the strength and frequency of the external force, respectively, and $\alpha\dddot{x}$ arises from the Abraham-Lorentz force present in plasmonic systems that describes the radiative loss.[17,18] By expressing the solution in the complex form as $x(\omega,t) = x_0(\omega)E_0e^{-i\omega t}$, the complex amplitude in steady state is given by

$$x_0(\omega) = \frac{1}{\omega_0^2 - \omega^2 - i\omega(\gamma + \omega^2\alpha)} \tag{6}$$

The dipole moment of the system is proportional to the amplitude of motion, $p_x = qE_0x_0(\omega)$. Substituting this into eq 1, we can express the backscattered far-field at distance h in the following form

$$E_x^{single}(\omega) = A\omega^2 x_0(\omega)e^{ikh}e^{i\phi} \tag{7}$$

where A is a factor depending on the strength of the driving field E_0 and the observation distance h; the propagation term e^{ikh} is taken into account and an additional phase correction ϕ is used for future convenience.

In general, disregarding the interband transitions of metals, this expression describes very well the far-field spectra of localized plasmonic resonances.[17] In Figure 2a, we plot the far-field amplitude and phase as a function of frequency for the single nanorod from the previous section. The value of phase is calculated in a way such that the propagation term e^{ikh} is subtracted. According to eq 7, the fitting curves for both amplitude and phase (solid lines in Figure 2a) match very well with the full electromagnetic SIE simulation (circular markers in Figure 2a): the residual of the least-square fit is as small as 5×10^{-3}. The fitting parameters are given in Table 1, and the phase correction ϕ is found to be zero. The fitting parameters are obtained using the least-squares solver in Matlab to find parameters the fit best to the problem, using a tolerance of 1×10^{-6}. The far-field scattering amplitude exhibits a broad resonance peak and the phase changes from 0 to π on crossing

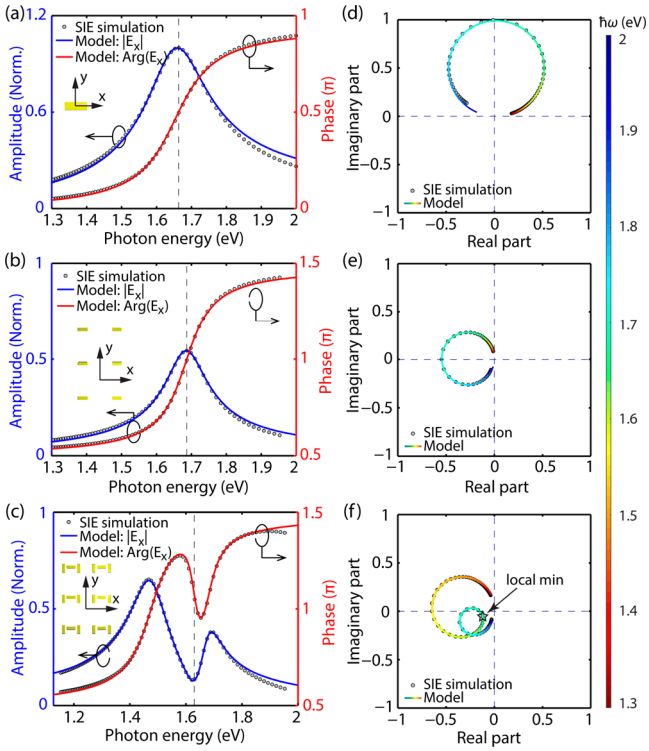

Figure 2. Amplitude and phase of the backscattering from (a) a single gold nanorod, (b) a subwavelength array of gold nanorods, and (c) a subwavelength array of gold nanodolmens. The schematics of the simulated systems are shown in the respective insets. (d), (e), and (f) plot the complex amplitude in the Argand plane for the situations in (a), (b), and (c), respectively. In all figures, circular markers denote values from electromagnetic SIE simulations, and the solid lines are best fits using the model.

Table 1. Fitting Parameters for Single Oscillator and Array of Identical Oscillators

	ω_0 (eV)	γ (eV)	α (eV)	ϕ (π)
single nanorod	1.663	0.019	0.055	0.0
periodic nanorods	1.689	0.019	0.034	0.51

the eigenfrequency. At the resonance condition when $\omega = \omega_0$, the corresponding phase is equal to $\pi/2$. In order to provide a better visualization of the complex electric field, we plot the complex amplitude as a curve parametrized by the frequency in the Argand plane (Figure 1d). The curve of the scattered field lies in the first and second quadrants.

On the other hand, the reflected field at a distance h from a periodic gold nanorod array can be calculated by substituting p_x into eq 4. One can again express the field in a simplified form

$$E_x^{array}(\omega) = A\omega x_0(\omega)e^{ikh}e^{i\phi} \tag{8}$$

where we expect a phase correction $\phi = \pi/2$ for a 2D square lattice.

Figure 2b shows the spectrum (in circular markers) of the nanorods array from the previous section and the fitting curve (in solid lines) using eq 8. The fitting parameters are listed in Table 1. The values of resonance frequency ω_0 and internal damping γ did not change significantly compared to those of a single nanorod. Radiative damping α decreases slightly. Most importantly, the phase correction parameter ϕ is now found to be 0.5π as expected. Note that the discrepancy at high

DOI: 10.1021/acsphotonics.6b00914
ACS Photonics 2017, 4, 852−860

Table 2. Fitting Parameters for Dolmen Arrays without Substrate, on Glass Substrate and on Gold Mirror with a Spacer

	ω_1 (eV)	ω_2 (eV)	γ_1 (eV)	γ_2 (eV)	α_1 (eV)	α_2 (eV)	κ (eV^2)	ϕ (π)
homogeneous medium	1.515	1.625	0.046	0.039	0.055	0	0.255	0.50
glass substrate	1.578	1.660	0.043	0.042	0.055	0	0.224	0.50
metallic backplane	1.486	1.610	0.124	0.048	0.020	0	0.240	0.51

frequency is mainly because the retardation effect becomes prominent when wavelength decreases, in which case the single oscillator with constant coupling coefficient approximation breaks down. In the Argand diagram (Figure 2e), it is clear that the curve is rotated counterclockwise by 90°. In the dipole approximation, such a phase correction can be applied to other periodic systems even when the unit cell has a complicated geometry, such as the plasmonic analogue of electromagnetically induced transparency (EIT), in which a bright dipole antenna element is coupled to a dark quadrupole antenna via near-field interaction.[20,21,32,36]

In this work we are interested in a metasurface that exhibits the plasmonic analogy of EIT, specifically, the dolmen structures shown in Figure 2c. The three nanorods have dimensions of 110 × 40 × 40 nm^3 and the gaps are each 10 nm. The coupling between the dipolar mode and the quadrupolar mode is tuned by the lateral displacement s of the dipolar antenna from the center position with s = 15 nm.[53] We first simulate an array with period $\Gamma_x = \Gamma_y$ = 400 nm in a homogeneous surrounding medium. The background refractive index for this plasmonic layer is again chosen to be $\bar{n}$ = 1.225. With incident polarization along x, the dipolar mode excited on the center nanorod couples with the quadrupolar mode supported by the two nanorods on the sides and results in a Fano-like line shape. Figure 2c shows the amplitude and phase of the reflected light calculated using SIE simulation. Briefly, the complex electric field is calculated at a point 50 μm away from the surface; then the phase is subtracted by removing the propagation term e^{ikh}. A dip in amplitude is observed at 1.62 eV that corresponds to the energy transfer to the quadrupolar dark mode. For the phase, the upswing around 1.51 eV is due to the dipolar resonance of the single nanorod, whereas the variation around 1.62 eV corresponds to the interference between the dipolar and quadrupolar resonances. This system can be described by the following coupled oscillator equations[18]

$$\ddot{x}_1 + \gamma_1\dot{x}_1 + \omega_1^2 x_1 + \kappa x_2 = \alpha_1\ddot{x}_1 + E_0 e^{-i\omega t}$$
$$\ddot{x}_2 + \gamma_2\dot{x}_2 + \omega_2^2 x_2 + \kappa x_1 = \alpha_2\ddot{x}_2 \quad (9)$$

where x_1 and x_2 are the amplitudes of bright and dark modes, and κ is the coupling coefficient. By expressing the solution for the radiative resonance in the form of $x_1(\omega,t) = x_b(\omega)E_0e^{-i\omega t}$, the complex amplitude in steady state becomes

$$x_b(\omega) = \frac{\omega_2^2 - \omega^2 - i\omega(\gamma_2 + \omega^2\alpha_2)}{-\kappa^2 + (\omega_1^2 - \omega^2 - i\omega(\gamma_1 + \omega^2\alpha_1))(\omega_2^2 - \omega^2 - i\omega(\gamma_2 + \omega^2\alpha_2))} \quad (10)$$

For a periodic array in a homogeneous medium, the far-field is again shifted by a phase of $\phi = \pi/2$. Similar to eq 8, the normalized reflection coefficient for such a plasmonic array can be expressed as

$$r_{\text{homo}}(\omega) = A\omega x_b(\omega)e^{ikh}e^{i\phi} \quad (11)$$

As shown in Figure 2c,f, eq 11 describes very well both the amplitude and phase of the normalized reflected field computed for an array of nanodolmens. The extracted parameters for the coupled oscillators model are given in Table 2. As expected for a dark mode, radiative damping coefficients α_2 of the second oscillator are much smaller than those of the first oscillator α_1, corresponding to the bright mode. The $\pi/2$ phase correction ϕ is still necessary since we are dealing here with an array. In the Argand diagram (Figure 2f), the frequency-dependent trace of the complex field in this coupled system exhibits an additional loop. This indicates that there exist two frequencies giving rise to exactly the same amplitude and phase. The minimum reflection, corresponding to EIT, occurs between these two frequencies as the loop approaches the origin (as indicated by the black star).

Effect of the Substrate. The analysis of mode frequency and coupling strength in periodic nanoresonators is essential in order to design metasurfaces with specific functionalities. Unfortunately, correct extraction of those parameters in complex optical environment remains difficult using conventional model. As soon as a substrate is introduced, the reflection spectrum from a metasurface is modified due to the resulting perturbation of the environment. Not only do the resonance frequencies shift, the lineshapes can also be different because of the additional interface. When the system is off-resonance, scattering from the plasmonic structures is minimal and one expects to observe the reflected field merely arising from the bare glass/air interface given by the Fresnel coefficient.[54] When the plasmonic array is on-resonance, the total reflected field is the summation of the light scattered from the plasmonic structures and that reflected from the glass/air interface. Depending on the phase relation between these two fields, the resonance features can either be enhanced or canceled.

To investigate the effect of the substrate, we simulate an array of gold dolmens with the same geometry as in the previous section, but now on a glass substrate with refractive index n_{glass} = 1.5, as illustrated in Figure 3a. The superstrate is air. Light is incident normally, first from the glass side, and excites the bright mode. The SIE calculated reflection amplitude and phase are shown with circular markers in Figure 3c. The resulting curves are different from the case in Figure 2c. Compared to the spectrum without substrate, the reflection dip in the case of a glass substrate is deeper and sharper. The phase now spans from 0.2π to 1.7π, with a more abrupt variation across the dark mode at 1.66 eV (without a substrate, the phase spanned from 0.1π to 0.9π, Figure 2a). The influence of the substrate is even more pronounced when we consider the system illustrated in Figure 3b, where the dolmen array is placed 40 nm above a semi-infinite gold substrate. The response of the system is shown in Figure 3d, where we now observe two dips in the reflected spectrum.

In addition to the resonance frequency shift, the substrate also changes dramatically the line shape and the phase of the reflection spectrum. In the absence of the substrate, these quantities could have been modeled very well using the coupled oscillator model as shown previously. We will show that the

DOI: 10.1021/acsphotonics.6b00914
ACS Photonics 2017, 4, 852−860

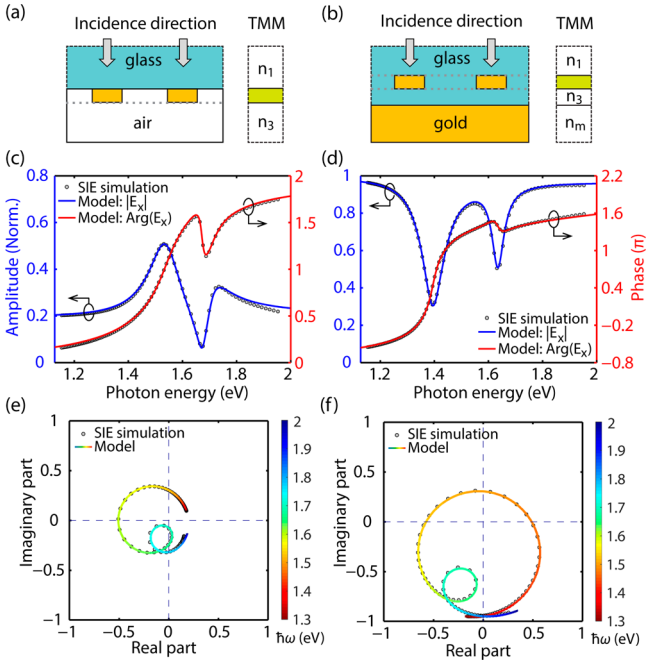

Figure 3. Schematics of a periodic plasmonic array (a) on a glass substrate with incident light along $+z$ and (b) above a gold substrate with a spacer of 40 nm and incident light along $-z$. (c) and (d) show the amplitude and phase of reflected fields for the situations in (a) and (b), respectively, and (e) and (f) plot the respective complex amplitudes in the Argand plane. In all figures, circular markers denote simulation values, and the solid lines are best fits using the model.

influence of the substrate can be incorporated by combining the oscillator model with the transfer matrix method (TMM).[55] In fact, the nanostructures placed in a homogeneous background that we have just investigated can be considered a special case of a planar stratified medium with three layers, where the superstrate and the substrate have the same refractive index and the plasmonic layer is sandwiched in between. The transfer matrix and the effective index of the plasmonic metasurface can be determined according to the reflection and transmission coefficients computed from the coupled oscillator model. Furthermore, knowing the effective medium parameters will allow deriving the reflection and transmission spectra of metasurfaces in other layered conditions, such as in the presence of glass or metallic substrates. In the actual model that we will introduce, it is unnecessary to find the exact effective index, since more complex layered structures eventually reduce to multiplying additional transfer matrices with the transfer matrix that accounts for the plasmonic layer.

Let us first derive the transfer matrix $\mathbf{M}_{\text{homo}}$ in the homogeneous background case. The system is divided into three layers: an incident medium with refractive index n_1; a middle layer including the plasmonic structures array (metasurfaces) with index n_2 and a final medium with index n_3, where $n_1 = n_3 = \bar{n}$. The system satisfies mirror symmetry about the plasmonic layer and one can write the total transfer matrix as

$$\mathbf{M}_{\text{homo}} = \frac{1}{t'}\begin{pmatrix} t'^2 - r'^2 & r' \\ -r' & 1 \end{pmatrix} \tag{12}$$

where the reflection coefficient $r' = r_{\text{homo}}(\omega)$ is given by the oscillator model according to eq 11, and the transmission coefficient is the sum of the incident field and the scattered field $t' = 1 + r'$.[38]

When the substrate is introduced, the incident medium index now differs from the substrate medium index $n \neq n_3$, and the total transfer matrix is the product of the matrix $\mathbf{M}^{\text{interf}}_{n_1/\bar{n}}$ for the first interface met by the incoming light, the homogeneous matrix $\mathbf{M}_{\text{homo}}$ and the matrix $\mathbf{M}^{\text{interf}}_{\bar{n}/n_3}$ for the second interface met by the light:

$$\mathbf{M} = \mathbf{M}^{\text{interf}}_{\bar{n}/n_3}\cdot\mathbf{M}_{\text{homo}}\cdot\mathbf{M}^{\text{interf}}_{n_1/\bar{n}} = \begin{pmatrix} M_{11} & M_{12} \\ M_{21} & M_{22} \end{pmatrix} \tag{13}$$

For normal incidence, the interface matrix between two media n_{in} and n_{out} is given by

$$\mathbf{M}^{\text{interf}}_{\text{in/out}} = \frac{1}{2n_{\text{out}}}\begin{pmatrix} n_{\text{out}} + n_{\text{in}} & n_{\text{out}} - n_{\text{in}} \\ n_{\text{out}} - n_{\text{in}} & n_{\text{out}} + n_{\text{in}} \end{pmatrix} \tag{14}$$

So the elements of the total transfer matrix are

$$M_{11} = \frac{(n_1 + n_3) + r'(n_1 + n_3 + 2\bar{n})}{2n_3 t'},$$

$$M_{12} = \frac{-(n_1 - n_3) - r'(n_1 - n_3 - 2\bar{n})}{2n_3 t'},$$

$$M_{21} = \frac{-(n_1 - n_3) - r'(n_1 - n_3 + 2\bar{n})}{2n_3 t'},$$

$$M_{22} = \frac{(n_1 + n_3) + r'(n_1 + n_3 - 2\bar{n})}{2n_3 t'} \tag{15}$$

Let us recall that $\bar{n}$ is the background media index used to compute the plasmonic layer. One can then calculate the total reflection and transmission coefficients from the system

$$r(\omega) = -\frac{M_{21}}{M_{22}} = \frac{(n_1 - n_3) + r_{\text{homo}}(n_1 - n_3 + 2\bar{n})}{(n_1 + n_3) + r_{\text{homo}}(n_1 + n_3 - 2\bar{n})} \tag{16}$$

and

$$t(\omega) = \frac{\det(\mathbf{M})}{M_{22}} = \frac{2n_1(1 + r_{\text{homo}})}{(n_1 + n_3) + r_{\text{homo}}(n_1 + n_3 - 2\bar{n})} \tag{17}$$

In the case of normal incidence from the glass side, $n_1 = 1.5$ and $n_3 = 1$, eq 11 does no longer describe the reflected field because of the presence of the substrate. However, the expression for the reflected field $r(\omega)$ in eq 16 fits exactly with the SIE simulation results in Figure 3c. The parameters extracted in that case for the coupled oscillators model are consistent with the parameters for the homogeneous medium, as shown in Table 2. The resonance frequencies ω_1 and ω_2 shift due to the presence of the substrate,[56] but the intrinsic properties such as internal damping coefficients γ_1 and γ_2, the radiative damping α_1 and α_2 and the coupling coefficient κ remain similar. In the Argand diagram (Figure 3e), the presence of the substrate modifies the complex reflected field observed for the homogeneous background in a way such that the entire curve scales up a little and is displaced toward the right (compare with Figure 2f). The loop becomes closer to the origin and, thus, the dark resonance dip ($\omega = 1.66$ eV) in the reflection spectrum appears closer to zero intensity. At off-resonance frequency ($\omega = 1.2$ or

DOI: 10.1021/acsphotonics.6b00914
ACS Photonics 2017, 4, 852−860

2 eV), the reflection coefficients remain constant at 0.2 in Figure 3c, which corresponds to the reflection from the glass/air interface.

Different substrates induce different effects on the reflection spectrum and this can be evaluated using the corresponding transfer matrix. For example, for the system illustrated in Figure 3b, one can derive the transfer matrix for the structure by considering 4 layers: a superstrate with refractive index n_1, a plasmonic layer, a spacer below with index n_3 and a gold substrate with index n_m given by the Drude model. The total transfer matrix can be written as

$$\mathbf{M} = \mathbf{M}^{\text{interf}}_{n_3/n_m} \cdot \mathbf{M}^{\text{prop}}_{n_3} \cdot \mathbf{M}^{\text{interf}}_{\overline{n}/n_3} \cdot \mathbf{M}_{\text{homo}} \cdot \mathbf{M}^{\text{interf}}_{n_1/\overline{n}} \tag{18}$$

with the interface matrices $\mathbf{M}^{\text{interf}}_{n_3/n_m}$ given by eq 14 and the propagation matrix $\mathbf{M}^{\text{prop}}_{n_3}$ given by

$$\mathbf{M}^{\text{prop}}_{n} = \begin{pmatrix} e^{i\varphi} & 0 \\ 0 & e^{-i\varphi} \end{pmatrix} \tag{19}$$

where $\varphi = 2\pi n d\omega/c$ is the propagation term within the spacer at normal incidence. For demonstration purpose, we chose $n_1 = n_3 = 1.5 = n_g$ in the full wave SIE simulation. After simplification, the reflection coefficient is then found to be

$$r(\omega) = \frac{(n_m + n_g) r_{\text{homo}} e^{-i\varphi} - (n_m - n_g)(2r_{\text{homo}} + 1) e^{i\varphi}}{(n_m + n_g) e^{-i\varphi} + r_{\text{homo}} (n_m - n_g) e^{i\varphi}} \tag{20}$$

Equation 20 fits extremely well with the electromagnetic SIE simulations (Figure 3d,f). The extracted parameters for the coupled oscillators model are shown in Table 2. These values do now systematically include the interaction between the metasurface and the metallic substrate by combining the TMM and the coupled oscillators model. For example, the presence of a gold mirror induces an opposite image dipole for each element in the metasurfaces, thus increasing the resonances losses. This effect results in a lower radiative damping coefficient α_1 and higher internal damping coefficients γ_1 and γ_2.

To further prove the validity of this model, we compare the transmission and reflection from the nanodolmen array on a glass substrate for the opposite incident conditions. At normal incidence from glass to air, the reflected field does not have a phase change with respect to the incident field, while the scattered field from the plasmonic array produces a phase shift of π ($\pi/2$ from the resonance condition and $\pi/2$ from the 2D periodic effect). This leads to destructive interference between the light scattered from the plasmonic structure and the light reflected from the glass/air interface. Thus, the total far-field in reflection is reduced to nearly zero at the dark resonance dip. On the other hand, reflection from air to glass is always accompanied by a phase flip of π, so that it is in-phase with the scattered field from the plasmonic structures; the total far-field intensity is stronger at the resonance in this case. The SIE simulation is shown as circular markers in Figure 4. The results have been fitted according to

$$R(\omega) = |r(\omega)|^2 \quad \text{and} \quad T(\omega) = \frac{n_3}{n_1} |t(\omega)|^2 \tag{21}$$

where $r(\omega)$ and $t(\omega)$ are from eqs 16 and 17, respectively, and n_1 and n_3 are the indices of input and output media (fitting curves are in blue for reflectance and in green for transmittance

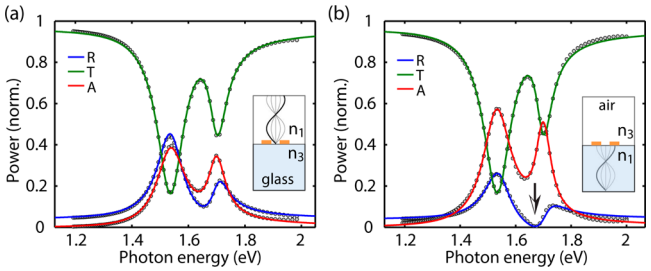

Figure 4. Normalized reflection (blue), transmission (green), and absorption (red) as a function of frequency for a nanodolmen array on a glass substrate with incident light from (a) the air side and (b) the glass side. Circular markers correspond to the SIE simulations and solid lines correspond to the curves obtained with eqs 16 and 17.

in Figure 4). In reflection, the dark resonance dip is not very pronounced for excitation from the air side (blue line in Figure 4a), while the dark resonance reflectance decreases to nearly zero at $\omega = 1.68$ eV for excitation from the glass side (blue line in Figure 4b). Transmittances are identical in Figure 4a,b because of reciprocity.[57] According to energy conservation, absorption given by $A = 1 - R - T$ is higher when light is incident from the glass side, since the plasmonic array is placed in the antinode of the electric field thanks to the zero phase change at the interface.[41]

Zero Reflection and Phase Bifurcation. The resulting near zero reflection in Figure 4b can enable phase flipping around that singularity frequency. Let us now restrict our study to the case of the glass substrate with incidence from the glass side in order to achieve a singular phase. Under this incidence condition, the phases of the scattered field and the reflected field from the interface are always opposite near the frequency of the dark resonance. In order to achieve exact zero reflection at this frequency, one needs to match the amplitudes of these two waves as well. One way is to vary the density of the plasmonic array in order to match the scattering intensity from the plasmonic array with the light reflected from the glass/air interface. Unfortunately, a large periodicity may result in higher diffraction orders and complicate the optical response.[21] The other possibility is to change the coupling strength between the dipolar mode and the quadrupolar mode, which effectively controls the intensity at the dark resonance frequency.[58]

In order to tune the coupling strength, we simulate nanodolmen metasurfaces with different lateral displacements of the center nanorod from $s = 0$ to 40 nm. Figure 5a presents the series of reflection spectra. When the structure is symmetric ($s = 0$), there is no coupling between the dipolar and quadrupolar modes, and the reflection spectrum exhibits a broad resonance peak. As the symmetry breaks, a dark resonance dip arises at 1.67 eV and the amplitude at the dip decreases with increasing coupling. We observe nearly zero reflection when $s = 20$ nm. The corresponding phase in Figure 5b shows an anomalous behavior: unlike the phase variation for low values of coupling, the phase changes from 0.2 to 3.8π across the resonances with an abrupt jump of π at 1.67 eV. In the Argand diagram (Figure 5c), larger nanorod displacements result in bigger loops since a stronger coupling splits the hybrid modes more. When $s = 20$ nm, the loop exactly passes through the origin, resulting in a phase flip of π. As the electric field amplitude has a winding number of two in the complex plane, the maximum phase change can be as large as 4π. The displacement $s = 20$ nm gives an optimum coupling strength to

DOI: 10.1021/acsphotonics.6b00914
ACS Photonics 2017, 4, 852−860

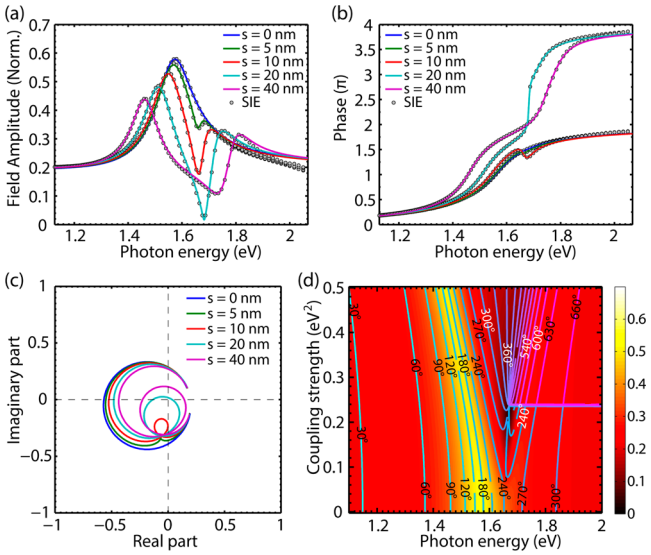

Figure 5. (a) Amplitude and (b) phase of reflection from a nanodolmen array on a glass substrate for different lateral displacements of the center nanorod from s = 0–40 nm. (c) Complex amplitude plotted in the Argand plane. (d) Reflection of light as a function of frequency and coupling strength calculated using the TMM together with the coupled oscillators model. The color map represents the amplitude, while the contour lines represent equiphase lines.

achieve zero reflection at ω = 1.67 eV. For s = 40 nm, the system becomes overcoupled and the amplitudes of the field scattered from the plasmonic layer and the field reflected from the interface do not match. Not only does the reflectance at the dip increase again, the phase also now varies smoothly across the resonance.

To further understand the dependence on coupling, we apply eq 16 and plot the amplitude of the reflected field as a function of frequency and coupling strength. The color map in Figure 5d illustrates the case of two coupled oscillators with intrinsic properties: ω_1 = 1.58, ω_2 = 1.66 eV, γ_1 = 0.043, γ_2 = 0.042 eV and α_1 = 0.055, α_2 = 0 eV. These two oscillators form the unit cell of a plasmonic array placed on a glass substrate. The blue and purple dashed lines indicate equiphase lines. When the frequency is ω = 1.67 eV and the coupling strength κ = 0.24 eV^2, the amplitude decreases to zero and the phase lines converge at this dislocation point. Note that the equiphase lines are discontinuous on the right-hand side of this singularity point exhibiting the phase jump between lower and higher coupling strength. In general, for super- and substrates with sufficient contrast in refractive indices, one can always find an optimum coupling strength to realize zero reflection and phase singularity.

Finally, as an application, we propose a sensing method based on the principle of phase discontinuity in such a metasurface. We fix the nanodolmens geometry with displacement s = 20 nm since the reflection approaches zero. Then, we change the refractive index of the superstrate from n = 1.112–1.12 RIU and probe the optical response. Figure 6a represents the phase profile around the sharp phase singularity frequency 1.61 eV. As the refractive index increases, not only does the position of the resonance red-shifts, the phase also exhibits a discontinuous jump. By fixing the excitation frequency at 1.61 eV, we plot the phase change at this frequency as a function of environment index in Figure 6b. The phase increases dramatically within a very small index range around 1.1165

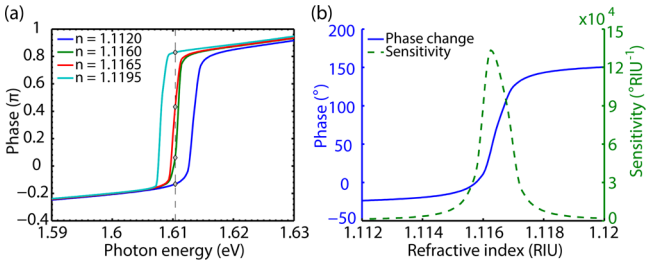

Figure 6. (a) Phase variation for the reflection from a nanodolmen array on a glass substrate as a function of frequency, close to the dark resonance dip for different background refractive indices. (b) Phase change and sensitivity as a function of refractive index at ω = 1.61 eV.

RIU, at which the sensitivity is as high as 135000° RIU^{-1} (green dashed line in Figure 6b). Compared to other sensors, this system benefits from the phase singularity and can, in principle, detect smaller changes.[59] This suggests that metasurfaces supporting dark resonances with both optimized coupling strength and environment feedback can be utilized to enhance the performance of sensors based on phase detection.[31] Practically, the coupling strength can be adjusted by either changing the incident angle or the polarization direction, depending on the system incorporated.

CONCLUSIONS

In conclusion, we have introduced a combined coupled oscillator/transfer matrix model that incorporates both periodicity and substrate effects to study the optical response of periodic plasmonic metasurfaces embedded in arbitrary stratified backgrounds, including metallic layers. While we have used the SIE method to retrieve the parameters of the coupled oscillators, any other numerical technique could have been utilized for that purpose[60] and combined with the TMM in a similar way. We have used this method to analyze the amplitude and phase of the reflection spectrum from a Fano-resonant metasurface and provided new insights into its dynamics by plotting it in the Argand plane. This method allows a better physical understanding of the light interaction within metasurfaces that can support several coupling channels. By utilizing the phase shifts introduced by the plasmonic metasurface and the substrates and adjusting the coupling strength, we have achieved zero reflection at the dark resonance frequency. This zero-reflection condition results in a spectral phase bifurcation of the reflected field, which enables high sensitivity phase-based sensing. Such phase bifurcations hold tremendous potential for sensing applications based on phase detection, which can possibly outperform conventional spectroscopic techniques.

ASSOCIATED CONTENT

Supporting Information

The Supporting Information is available free of charge on the ACS Publications website at DOI: 10.1021/acsphotonics.6b00914.

Comparison between SIE and FDTD; Fine-tuning around singularity condition (PDF).

AUTHOR INFORMATION

Corresponding Author

*E-mail: olivier.martin@epfl.ch.

DOI: 10.1021/acsphotonics.6b00914
ACS Photonics 2017, 4, 852–860

ORCID

Chen Yan: 0000-0002-3171-0449
T. V. Raziman: 0000-0002-7085-6934
Olivier J. F. Martin: 0000-0002-9574-3119

Funding

Funding from the European Research Council (ERC-2015-AdG-695206 Nanofactory) and from the Swiss National Science Foundation (Projects 200021_162453 and 200020_135452) are gratefully acknowledged.

Notes

The authors declare no competing financial interest.

REFERENCES

(1) Anker, J. N.; Hall, W. P.; Lyandres, O.; Shah, N. C.; Zhao, J.; Van Duyne, R. P. Biosensing with plasmonic nanosensors. *Nat. Mater.* **2008**, *7*, 442−453.

(2) Liu, N.; Liu, H.; Zhu, S. N.; Giessen, H. Stereometamaterials. *Nat. Photonics* **2009**, *3*, 157−162.

(3) Yu, N.; Genevet, P.; Kats, M. A.; Aieta, F.; Tetienne, J.-P.; Capasso, F.; Gaburro, Z. Light Propagation with Phase Discontinuities: Generalized Laws of Reflection and Refraction. *Science* **2011**, *334*, 333−337.

(4) Wu, C.; Khanikaev, A. B.; Adato, R.; Arju, N.; Yanik, A. A.; Altug, H.; Shvets, G. Fano-resonant asymmetric metamaterials for ultrasensitive spectroscopy and identification of molecular monolayers. *Nat. Mater.* **2011**, *11*, 69−75.

(5) Kauranen, M.; Zayats, A. V. Nonlinear plasmonics. *Nat. Photonics* **2012**, *6*, 737−748.

(6) Zheludev, N. I.; Kivshar, Y. S. From metamaterials to metadevices. *Nat. Mater.* **2012**, *11*, 917−924.

(7) Roy, T.; Rogers, E. T. F.; Zheludev, N. I. Sub-wavelength focusing meta-lens. *Opt. Express* **2013**, *21*, 7577−7582.

(8) Metzger, B.; Schumacher, T.; Hentschel, M.; Lippitz, M.; Giessen, H. Third Harmonic Mechanism in Complex Plasmonic Fano Structures. *ACS Photonics* **2014**, *1*, 471−476.

(9) Yu, N.; Capasso, F. Flat optics with designer metasurfaces. *Nat. Mater.* **2014**, *13*, 139−150.

(10) Zhang, Y.; Zhen, Y.-R.; Neumann, O.; Day, J. K.; Nordlander, P.; Halas, N. J. Coherent anti-Stokes Raman scattering with single-molecule sensitivity using a plasmonic Fano resonance. *Nat. Commun.* **2014**, *5*, 4424.

(11) Minovich, A. E.; Miroshnichenko, A. E.; Bykov, A. Y.; Murzina, T. V.; Neshev, D. N.; Kivshar, Y. S. Functional and nonlinear optical metasurfaces. *Laser Photonics Rev.* **2015**, *9*, 195−213.

(12) King, N. S.; Liu, L.; Yang, X.; Cerjan, B.; Everitt, H. O.; Nordlander, P.; Halas, N. J. Fano Resonant Aluminum Nanoclusters for Plasmonic Colorimetric Sensing. *ACS Nano* **2015**, *9*, 10628−10636.

(13) Butet, J.; Yang, K.-Y.; Dutta-Gupta, S.; Martin, O. J. F. Maximizing Nonlinear Optical Conversion in Plasmonic Nanoparticles through Ideal Absorption of Light. *ACS Photonics* **2016**, *3*, 1453−1460.

(14) Joe, Y. S.; Satanin, A. M.; Kim, C. S. Classical analogy of Fano resonances. *Phys. Scr.* **2006**, *74*, 259−266.

(15) Christ, A.; Ekinci, Y.; Solak, H. H.; Gippius, N. A.; Tikhodeev, S. G.; Martin, O. J. F. Controlling the Fano interference in a plasmonic lattice. *Phys. Rev. B: Condens. Matter Mater. Phys.* **2007**, *76*, 201405.

(16) Zuloaga, J.; Nordlander, P. On the Energy Shift between Near-Field and Far-Field Peak Intensities in Localized Plasmon Systems. *Nano Lett.* **2011**, *11*, 1280−1283.

(17) Kats, M. A.; Yu, N.; Genevet, P.; Gaburro, Z.; Capasso, F. Effect of radiation damping on the spectral response of plasmonic components. *Opt. Express* **2011**, *19*, 21748−21753.

(18) Lovera, A.; Gallinet, B.; Nordlander, P.; Martin, O. J. F. Mechanisms of fano resonances in coupled plasmonic systems. *ACS Nano* **2013**, *7*, 4527−4536.

(19) Giannini, V.; Francescato, Y.; Amrania, H.; Phillips, C. C.; Maier, S. A. Fano Resonances in Nanoscale Plasmonic Systems: A Parameter-Free Modeling Approach. *Nano Lett.* **2011**, *11*, 2835−2840.

(20) Gallinet, B.; Martin, O. J. F. Ab initio theory of Fano resonances in plasmonic nanostructures and metamaterials. *Phys. Rev. B: Condens. Matter Mater. Phys.* **2011**, *83*, 235427.

(21) Yan, C.; Martin, O. J. F. Periodicity-Induced Symmetry Breaking in a Fano Lattice: Hybridization and Tight-Binding Regimes. *ACS Nano* **2014**, *8*, 11860−11868.

(22) Abelès, F. Surface electromagnetic waves ellipsometry. *Surf. Sci.* **1976**, *56*, 237−251.

(23) Ghim, Y.-S.; Suratkar, A.; Davies, A. Reflectometry-based wavelength scanning interferometry for thickness measurements of very thin wafers. *Opt. Express* **2010**, *18*, 6522−6529.

(24) Abdulhalim, I. Spatial and temporal coherence effects in interference microscopy and full-field optical coherence tomography. *Ann. Phys.* **2012**, *524*, 787−804.

(25) Kravets, V. G.; Schedin, F.; Jalil, R.; Britnell, L.; Gorbachev, R. V.; Ansell, D.; Thackray, B.; Novoselov, K. S.; Geim, A. K.; Kabashin, A. V.; Grigorenko, A. N. Singular phase nano-optics in plasmonic metamaterials for label-free single-molecule detection. *Nat. Mater.* **2013**, *12*, 304−309.

(26) Claus, D.; Robinson, D. J.; Chetwynd, D. G.; Shuo, Y.; Pike, W. T.; José, J. D. J. T. G.; Rodenburg, J. M. Dual wavelength optical metrology using ptychography. *J. Opt.* **2013**, *15*, 035702.

(27) Homola, J. Surface Plasmon Resonance Sensors for Detection of Chemical and Biological Species. *Chem. Rev.* **2008**, *108*, 462−493.

(28) Kravets, V. G.; Schedin, F.; Kabashin, A. V.; Grigorenko, A. N. Sensitivity of collective plasmon modes of gold nanoresonators to local environment. *Opt. Lett.* **2010**, *35*, 956−958.

(29) Cao, Z. L.; Wong, S. L.; Wu, S. Y.; Ho, H. P.; Ong, H. C. High performing phase-based surface plasmon resonance sensing from metallic nanohole arrays. *Appl. Phys. Lett.* **2014**, *104*, 1−5.

(30) Maier, S. A. *Plasmonics: Fundamentals and Applications*; Springer, 2007.

(31) Svedendahl, M.; Verre, R.; Kall, M. Refractometric biosensing based on optical phase flips in sparse and short-range-ordered nanoplasmonic layers. *Light: Sci. Appl.* **2014**, *3*, e220.

(32) Zhang, S.; Genov, D. A.; Wang, Y.; Liu, M.; Zhang, X. Plasmon-induced transparency in metamaterials. *Phys. Rev. Lett.* **2008**, *101*, n/a.

(33) Miroshnichenko, A. E.; Flach, S.; Kivshar, Y. S. Fano resonances in nanoscale structures. *Rev. Mod. Phys.* **2010**, *82*, 2257−2298.

(34) Sonnefraud, Y.; Verellen, N.; Sobhani, H.; Vandenbosch, G. A. E.; Moshchalkov, V. V.; Van Dorpe, P.; Nordlander, P.; Maier, S. A. Experimental Realization of Subradiant, Superradiant, and Fano Resonances in Ring/Disk Plasmonic Nanocavities. *ACS Nano* **2010**, *4*, 1664.

(35) Luk'yanchuk, B.; Zheludev, N. I.; Maier, S. A.; Halas, N. J.; Nordlander, P.; Giessen, H.; Chong, C. T. The Fano resonance in plasmonic nanostructures and metamaterials. *Nat. Mater.* **2010**, *9*, 707−715.

(36) Francescato, Y.; Giannini, V.; Maier, S. A. Plasmonic Systems Unveiled by Fano Resonances. *ACS Nano* **2012**, *6*, 1830−1838.

(37) Auguie, B.; Bendana, X. M.; Barnes, W. L.; Garcia de Abajo, F. J. Diffractive arrays of gold nanoparticles near an interface: Critical role of the substrate. *Phys. Rev. B: Condens. Matter Mater. Phys.* **2010**, *82*, 155447.

(38) D'Aguanno, G.; Mattiucci, N. Dispersive and scattering properties of multilayer arrays made of plasmonic nanoparticles. *J. Opt. Soc. Am. B* **2014**, *31*, 2524−2530.

(39) Lévêque, G.; Martin, O. J. F. Optical interactions in a plasmonic particle coupled to a metallic film. *Opt. Express* **2006**, *14*, 9971−9981.

(40) Zhang, S.; Bao, K.; Halas, N. J.; Xu, H.; Nordlander, P. Substrate-Induced Fano Resonances of a Plasmonic Nanocube: A Route to Increased-Sensitivity Localized Surface Plasmon Resonance Sensors Revealed. *Nano Lett.* **2011**, *11*, 1657−1663.

(41) Ameling, R.; Giessen, H. Cavity Plasmonics: Large Normal Mode Splitting of Electric and Magnetic Particle Plasmons Induced by a Photonic Microcavity. *Nano Lett.* **2010**, *10*, 4394−4398.

DOI: 10.1021/acsphotonics.6b00914
ACS Photonics 2017, 4, 852−860

(42) Esfandyarpour, M.; Garnett, E. C.; Cui, Y.; McGehee, M. D.; Brongersma, M. L. Metamaterial mirrors in optoelectronic devices. *Nat. Nanotechnol.* **2014**, *9*, 542−547.
(43) Pinchuk, A.; Hilger, A.; Plessen, G. v.; Kreibig, U. Substrate effect on the optical response of silver nanoparticles. *Nanotechnology* **2004**, *15*, 1890.
(44) Dmitriev, A.; Hagglund, C.; Chen, S.; Fredriksson, H.; Pakizeh, T.; Kall, M.; Sutherland, D. S. Enhanced Nanoplasmonic Optical Sensors with Reduced Substrate Effect. *Nano Lett.* **2008**, *8*, 3893−3898.
(45) Moreno, F.; García-Cámara, B.; Saiz, J. M.; González, F. Interaction of nanoparticles with substrates: effects on the dipolar behaviour of the particles. *Opt. Express* **2008**, *16*, 12487−12504.
(46) Paulus, M.; Gay-Balmaz, P.; Martin, O. J. F. Accurate and efficient computation of the Green's tensor for stratified media. *Phys. Rev. E: Stat. Phys., Plasmas, Fluids, Relat. Interdiscip. Top.* **2000**, *62*, 5797−807.
(47) Yatsenko, V.; Maslovski, S.; Tretyakov, S. Electromagnetic Interaction of Parallel Arrays of Dipole Scatterers. *Journal of Electromagnetic Waves and Applications* **2000**, *14*, 79−82.
(48) Kern, A. M.; Martin, O. J. F. Surface integral formulation for 3D simulations of plasmonic and high permittivity nanostructures. *J. Opt. Soc. Am. A* **2009**, *26*, 732−740.
(49) Raziman, T. V.; Somerville, W. R. C.; Martin, O. J. F.; Le Ru, E. C. Accuracy of surface integral equation matrix elements in plasmonic calculations. *J. Opt. Soc. Am. B* **2015**, *32*, 485−492.
(50) Gallinet, B.; Martin, O. J. F. Scattering on plasmonic nanostructures arrays modeled with a surface integral formulation. *Photonics Nanostruct. Fundam. Appl.* **2010**, *8*, 278−284.
(51) Oubre, C.; Nordlander, P. Optical Properties of Metallodielectric Nanostructures Calculated Using the Finite Difference Time Domain Method. *J. Phys. Chem. B* **2004**, *108*, 17740−17747.
(52) Stockman, M. I. Nanoplasmonics: past, present, and glimpse into future. *Opt. Express* **2011**, *19*, 22029−22106.
(53) Gallinet, B.; Martin, O. J. F. Refractive Index Sensing with Subradiant Modes: A Framework To Reduce Losses in Plasmonic Nanostructures. *ACS Nano* **2013**, *7*, 6978−6987.
(54) Saleh, B. E. A.; Teich, M. C., Electromagnetic Optics. In *Fundamentals of Photonics*; John Wiley & Sons, Inc., 2001; pp 157−192.
(55) Hecht, E. *Optics*; Addison-Wesley, 2002.
(56) Fischer, H.; Martin, O. J. F. Engineering the optical response of plasmonic nanoantennas. *Opt. Express* **2008**, *16*, 9144−9154.
(57) Agarwal, G. S.; Gupta, S. D. Reciprocity relations for reflected amplitudes. *Opt. Lett.* **2002**, *27*, 1205−1207.
(58) Gallinet, B.; Siegfried, T.; Sigg, H.; Nordlander, P.; Martin, O. J. F. Plasmonic Radiance: Probing Structure at the Angstrom Scale with Visible Light. *Nano Lett.* **2013**, *13*, 497−503.
(59) Bahramipanah, M.; Dutta-Gupta, S.; Abasahl, B.; Martin, O. J. F. Cavity-Coupled Plasmonic Device with Enhanced Sensitivity and Figure-of-Merit. *ACS Nano* **2015**, *9*, 7621−7633.
(60) Gallinet, B.; Butet, J.; Martin, O. J. F. Numerical methods for nanophotonics: standard problems and future challenges. *Laser Photon. Rev.* **2015**, *9*, 577−603.

DOI: 10.1021/acsphotonics.6b00914
ACS Photonics 2017, 4, 852−860